Youcefi *et al.*
*Chinese Journal of Mechanical Engineering* (2023) 36:147
https://doi.org/10.1186/s10033-023-00981-8

Chinese Journal of Mechanical Engineering

ORIGINAL ARTICLE

Open Access

# Effect of an Inclined Slots on the Power Consumption and Vortices Size in a Rushton Turbine Agitated Tank

Sarra Youcefi[1*], Mohamed Bouzit[2], Abdelkader Youcefi[3] and Abderrahim Mokhefi[4]

**Abstract**

Mechanical agitation in baffled vessels with turbines plays a vital role in achieving homogeneous fluid mixing and promoting various transfer operations. Therefore, designing vessels with optimal energy efficiency and flow dynamics is essential to enhance operational performance and eliminate flow perturbations. Hence, the present research focuses on a numerical investigation of the impact of inclined slots with different angles installed at the sidewall of a cylindrical vessel equipped with a Rushton turbine. This study explores power consumption and vortex size while considering various rotation directions of the impeller with different rotation speeds. The numerical simulations are conducted for Reynolds numbers ranging from $10^4$ to $10^5$, using the RANS *k-ε* turbulence model to govern the flow inside the stirred vessel, accounting for mass and momentum balances. The results have shown that the installation of slots reduces power consumption and vortex size compared to conventional vessel configurations. Moreover, increasing the slot angle from 0 to 32.5° further reduces energy consumption and vortex size, especially with negative rotation speeds. On the other hand, increasing the Reynolds numbers leads to a decrease in power consumption and an increase in vortex size. The present research therefore proposes a design for constructing Rushton-turbine stirred vessels offering optimal operation, characterized by reduced energy consumption and minimized vortex size.

**Keywords** Mixing, Stirred tank, Rushton turbine, Inclined slots, Hydrodynamic, Power consumption, Vortices size

## 1 Introduction

Mixing is the most common process in chemical, biochemical, pharmaceutical, polymer, mineral, food and wastewater treatment industries. Such processes are strongly influenced by the hydrodynamic, turbulent flow conditions and mixing characteristics. Many experimental and theatrical investigations were conducted on the hydrodynamics behavior of mixing processes in vessels of various geometrical configurations, equipped with different types of impellers and filled with different fluid rheology [1–4].

During the last three decades, computational fluid dynamics (CFD) has become an important tool for understanding flow phenomena. The capability of CFD tools for predicting mixing behavior in terms of mixing time, power consumption, flow pattern and velocity

*Correspondence:
Sarra Youcefi
sarra.youcefi@univ-usto.dz
[1] Laboratory of Applied Mechanics, Department of Mechanical Engineering, University of Sciences and Technology of Oran, Oran 31000, Algeria
[2] Laboratory of Maritime Sciences and Engineering, Department of Marine Engineering, University of Science and Technology of Oran, Oran 31000, Algeria
[3] Laboratory of Aeronautics and Propulsion Systems, Department of Mechanical Engineering, University of Science and Technology of Oran, Oran 31000, Algeria
[4] Laboratory of Mechanics, Modeling and Experimentation, Department of Mechanical Engineering, Tahri Mohamed University of Bechar, Bechar 08000, Algeria

profiles is considered as a successful achievement of these methods, which proven acceptable results [5]. Ng and Yianneskis [6] used the CFD predictions of the flow using a sliding mesh technique in the stirred vessel and Rushton turbine. The large-eddy simulation (LES) is one of the most powerful turbulence models in CFD. It was also present in the case of mechanical agitation in cylindrical tanks. Zadghaffari et al. [7] considered this model to predict the flow field, power consumption, mixing time, turbulent kinetic energy and turbulent dissipation rate. They found that the stirring power increase by increasing the rotation speed of the turbine.

As agitation process is very important, researchers in this domain have mainly focused on CFD and experimental studies to improve the hydrodynamic performance in the presence of various types of fluids including complex fluids, suspensions and nanofluids [8–11]. Wang et al. [12] presented the results of the power consumption required to suspend water-solids slurries in a mechanically agitated vessel. It has been concluded that improving solids suspensions could be achieved by removing baffles. In addition, the impacts of solid concentration and particle size on power consumption have been also investigated. The analysis of the mixing time inside the agitated tanks was strongly present in the research field. On the other hand, Youcefi et al. [13] experimentally studied the mixing time of a two-blade stirrer during mixing of viscoelastic fluids. They found that the mixing time strongly depended on the viscoelasticity of the solutions.

Mainly, Rushton turbines are used to promote gas/liquid exchange and dispersion by centrifugal effect. On the other hand, due to their high rotational speed, they are designed for mixing and homogenizing products that require a low shear rate. In this regard, in the context of improving the performance of the turbine and the resulting flow, researchers in the field of mechanical agitation and mixing are making geometric modifications to their blades, diameter, and disposition. Taghavi et al. [14] investigated the power consumption of a stirred tank equipped with dual Rushton impellers in both single phase and gas-liquid phases. The results were validated using both experimental and simulation data. Foukrach et al. [15] compared the effect of different types of turbines on the energy consumption and the vortex size. They showed that the converging triangular blade turbine type gives a significant gain on energy consumption. On the other hand, the diverging triangular blade turbine type gives a good reduction in vortex size. The effect of the turbine clearance has been analyzed in the works of Karcz and Major [16] and Yapici et al. [17]. They reported that the power number decreases with the decrease of the clearance of the turbine from the bottom of the vessel and with the increase of the disc thickness. Beloudane et al. [18] investigated the effect of blade shape on flow patterns in a stirred tank. Their proposed converging hollow blade design resulted in highly radial flows, increasing radial velocity by 35% with lower power consumption compared to the flat blade. Hassouni et al. [19] numerically investigated impeller rotational motion and thermal buoyancy in a mechanical mixer. They demonstrated that the Richardson number had no effect on the power number, but thermal buoyancy impacted fluid mixing quality. Jia et al. [20] developed improved disc turbines to reduce power consumption and improve mixing in stirred tanks. Compared to traditional system, they obtained a 43% power reduction and 68% higher pumping efficiency. Jenish et al. [21] demonstrated that utilizing four-bladed Rushton turbines at eight angles allows finding an optimal power level without compromising radial flow patterns. Zhang et al. [22] investigated the laminar-turbulent transition of single-phase flow around a Rushton turbine impeller in a stirred tank experimentally and computationally.

The use of baffles in agitated tanks favors to reduce the vortices size in the liquid. It promotes the circulation between the top and bottom of the tank. On the other hand, these baffles allow to a very important energy consumption in side ther stirred system, thus reducing mixing time. In industrial installations, baffles are used in cylindrical tanks, especially where the viscosity of the mixture is not high as well as the mixing intensity is not low. Many numerical and experimental investigations are carried out on the behavior of agitated liquid inside baffled stirred tanks and vessels. Roy et al. [23] carried out a numerical study in a baffled tank with inclined blades in a turbulent regime, using LES simulation. They showed that in the case of perturbation, the average power input is 18% higher than in the fixed regime. Ammar et al. [24] examined the effect of baffle length on turbulent flow in a tank agitated by a Rushton turbine using the MRF method in the turbulent regime. Under these conditions, the power number is highly dependent on baffle length. Bittins and Zehner [25] studied the dynamic interaction between the agitation tool and baffle within vessel equipped by a radial flow agitator. They also studied and compared the power consumption number as function of diameter ratio. Bhattacharya et al. [26] studied air entrainment in baffled stirred tanks. They showed that baffles can significantly impact the flow patterns and air entrainment in stirred tanks. Fan et al. [27] studied the impact of baffles on flow structure and cyclic variation in stirred tanks with Rushton turbines using particle image velocimetry. They showed that baffles increased time-averaged velocity peaks, enlarged high-velocity regions, and enhanced fluid element fluctuations near the turbine.

Tamburini et al. [28] conducted RANS simulations of laboratory scale unbaffled and baffled tanks stirred by a Rushton turbine using three turbulence models. In the baffled vessel, no significant differences were observed among the predictions of the three models. Results were validated against experimental data and DNS simulations. Youcefi et al. [29] studied the influence of several configurations of agitated vessel using Rushton turbine with six straight blades namely: baffled vessel, unbaffled vessel and vessel with slots, in order to determine the velocity profile, energy consumption as well as the size of vortex. They showed that the location of slots in the vessel allowed the reduction in vortex size and decreasing the energy consumption. Shabani et al. [30] showed that role of baffles in a mechanically agitated vessel is to ensure even distribution, reduce settler turbulence, promote the stability of power drawn by the impeller, prevent liquids swirling and vortex formation. Kamla et al. [31, 32] numerically reduced the energy consumption and the vortices size in Rushton turbine agitated vessel through new incurved and inclined baffles. Foukrach and Ameur [33] numerically analyzed the effect of the baffle curvature, their length, width as well as position in a turbine stirred tank, and on the hydrodynamic behavior and power consumption. Their investigation revealed that the curved shape allows for a wider well-agitated region and a more powerful radial fluid jet than straight baffles. Other recent works have been conducted in Refs. [34–36] on Rushton turbines, including RANS simulations of laboratory-scale tanks, both with unbaffled and baffled configurations, to study performance and flow behavior under different turbulence conditions.

The comparative analysis of previous numerical and experimental works, by conducting many researches on this subject, allows to confirm the important role of baffles and slots installation on the flow of fluids in stirred tanks, particularly on the reduction of the vortices size. Moreover, in this case, the stirring power consumption is strongly affected. In order to further improve the characteristics of mechanical stirring induced by Rushton turbines, the present paper, gives a numerical investigation of the effect of inclined slots installed on an agitated vessel sidewall on the flow behavior and energy consumption. To give a best knowledge, the inertia effect, turbine rotation direction as well as the inclination angle have been highlighted on the agitated system behavior. It should be noted, that this installation of inclined slots has not been previously studied in the literature of agitation and mixing, hence, it represents the original motivation of the present work.

## 2 Geometrical Presentation

The stirred system consists of a cylindrical tank of diameter $D$ with a flat bottom, see Figure 1. The liquid level $H$ is equal to the diameter of the vessel. This tank is equipped with a standard Rushton turbine with six blades of a diameter $d$. These blades are mounted on a disk of diameter $\delta$ and thickness $th$ where the clearance between the bottom of the vessel and the midsection of this disc is $c$. The length and width of each blade are respectively $a$ and $h$. The turbine disk is connected with a shaft of diameter $b$. The cylindrical tank is equipped with four inclined slots of a width $E$ and a length $F$ for different inclination angles $\alpha = 0°$, 10°, 22.5° and 32.5°, see Figure 2.

The geometrical ration used in the present work are: $H/D = 1$, $d/D = 1/3$, $\delta/d = 3/4$, $th/d = 2/50$, $c/D = 1/3$, $a/d = 1/4$, $h/d = 1/5$, $b/d = 1/5$, $F/D = 1/5$, $E/D = 1/15$.

The water at 25 °C where the density and the dynamic viscosity are respectively equal to 997 kg/m$^3$ and 0.00089 Pa·s, has been used as the working fluid.

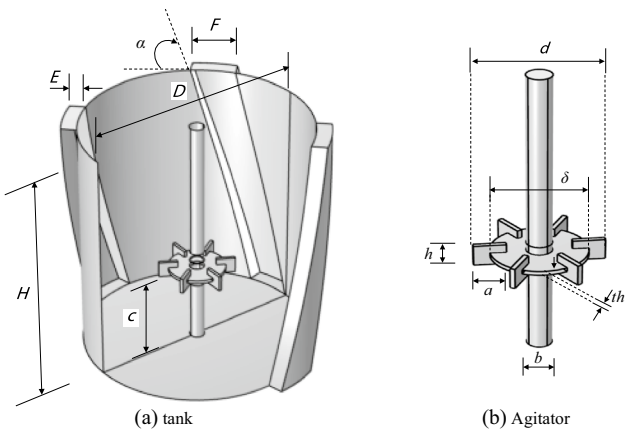


(a) tank (b) Agitator

**Figure 1** Stirred vessel equipped with inclined slots

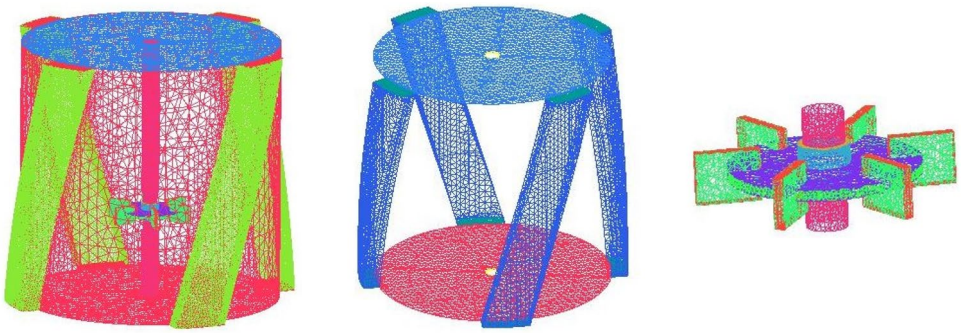

(a) (b) (c)

**Figure 2** Mesh of the agitated system: (**a**) Mesh of the entire domain, (**b**) Sots mesh, (**c**) Turbine mesh

## 3 Governing Equations

### 3.1 Dimensional Governing Equations

The turbulent flow in the agitated vessel is governed by the equations describing the mass and momentum balance. The standard *k*-*ε* model has been retained to solve the term of Reynolds stress-appearing in the momentum equation. Thus, in three-dimensional frame, these governing balances are:

mass balance:

$$\frac{\partial \rho}{\partial t}+\frac{\partial(\rho u_j)}{\partial x_j}=0, \tag{1}$$

momentum balance:

$$\frac{\partial(\rho u_i)}{\partial t}+\frac{\partial(\rho u_j u_i)}{\partial x_j}=-\frac{\partial p}{\partial x_i}+\frac{\partial}{\partial x_j}\left[(\mu+\mu_t)\left(\frac{\partial u_i}{\partial x_j}+\frac{\partial u_j}{\partial x_i}\right)\right]-\rho g, \tag{2}$$

kinetic energy balance:

$$\frac{\partial(\rho k)}{\partial t}+\frac{\partial(\rho u_i k)}{\partial x_i}=\frac{\partial}{\partial x_i}\left(\mu+\frac{\mu_t}{\sigma_k}\right)\frac{\partial k}{\partial x_i}+P_k-\rho\varepsilon, \tag{3}$$

dissipation rate of turbulence balance:

$$\frac{\partial(\rho\varepsilon)}{\partial t}+\frac{\partial(\rho u_i \varepsilon)}{\partial x_i}=\frac{\partial}{\partial x_i}\left(\mu+\frac{\mu_t}{\sigma_\varepsilon}\right)\frac{\partial \varepsilon}{\partial x_i}+C_{\varepsilon 1}\frac{\varepsilon}{k}P_k-C_{\varepsilon 2}\rho\frac{\varepsilon^2}{k}. \tag{4}$$

The turbulent viscosity appearing in Eqs. (1)–(4) is defined by the following expression:

$$\mu_t=\rho C_\mu\frac{k^2}{\varepsilon}. \tag{5}$$

The generation term appearing in Eq. (3) and Eq. (4) is given by:

$$P_k=\mu_t\left(\frac{\partial u_i}{\partial x_j}+\frac{\partial u_i}{\partial x_i}\right)\frac{\partial u_j}{\partial x_i}. \tag{6}$$

The following constants of the standard *k*-*ε* model has been used: $C_\mu = 0.09$, $C_{\varepsilon 1} = 1.44$, $C_{\varepsilon 2}= 1.92$, $\sigma_k = 1$, $\sigma_\varepsilon = 1.314$.

### 3.2 Dimensionless Governing Equations

The dimensionless equations that govern the turbulent flow inside the agitated medium are obtained by the substitution of a set of dimensionless variables in Eqs. (1)–(6). These variables are defined by:

$$\tau=2\pi Nt, X_i=\frac{2x_i}{D}, U_i=\frac{u_i}{\pi ND}, P_i=\frac{p_i}{\rho(\pi ND)^2},\quad \overline{k}=\frac{k}{(\pi ND)^2}\ \text{and}\ \overline{\varepsilon}=\frac{\varepsilon D}{2(\pi ND)^3}. \tag{7}$$

The dimensionless governing system Eqs. (1)–(4) become:

dimensionless masse balance:

$$\frac{\partial U_j}{\partial X_j}=0, \tag{8}$$

dimensionless momentum balance:

$$\frac{\partial(U_i)}{\partial \tau}+\frac{\partial(U_j U_i)}{\partial X_j}=-\frac{\partial P}{\partial X_i}+\frac{2}{\pi}\left(\frac{d}{D}\right)^2\frac{1}{Re}\frac{\partial}{\partial X_j}\times\left[\left(1+\frac{\overline{\mu}_t}{\mu}\right)\left(\frac{\partial U_i}{\partial X_j}+\frac{\partial U_j}{\partial X_i}\right)\right]-\frac{1}{Fr}, \tag{9}$$

dimensionless kinetic energy balance:

$$\frac{\partial \overline{k}}{\partial \tau}+\frac{\partial (U_i \overline{k})}{\partial X_i}=\frac{2}{\pi}\left(\frac{d}{D}\right)^2\frac{1}{Re}\frac{\partial}{\partial X_i}\left(1+\frac{\mu_t}{\sigma_k \mu}\right)\frac{\partial \overline{k}}{\partial X_i}+\overline{P}_k-\overline{\varepsilon}, \tag{10}$$

dimensionless dissipation rate of turbulence balance:

$$\frac{\partial \overline{\varepsilon}}{\partial \tau}+\frac{\partial U_i \overline{\varepsilon}}{\partial X_i}=\frac{2}{\pi}\left(\frac{d}{D}\right)^2\frac{1}{Re}\frac{\partial}{\partial X_i}\left(1+\frac{\mu_t}{\sigma_\varepsilon \mu}\right)\frac{\partial \overline{\varepsilon}}{\partial x_i}+C_{\varepsilon 1}\frac{\overline{\varepsilon}}{\overline{k}}P_k-C_{\varepsilon 2}\frac{\overline{\varepsilon}^2}{\overline{k}}. \tag{11}$$

The dimensionless turbulent viscosity is defined by:

$$\overline{\mu}_t=C_\mu\frac{\overline{k}^2}{\overline{\varepsilon}}. \tag{12}$$

The dimensionless generation term is given by:

$$P_k=\overline{\mu}_t\left(\frac{\partial U_i}{\partial X_j}+\frac{\partial U_i}{\partial X_i}\right)\frac{\partial U_j}{\partial X_i}. \tag{13}$$

The dimensionless numbers namely: Reynolds number and Froude number appear in the set of the dimensionless Eqs. (8)−(11). These numbers are respectively defined by:

$$Re=\frac{\rho N d^2}{\mu}, \tag{14}$$

$$Fr=\frac{g}{2(\pi N)^2 D}. \tag{15}$$

### 3.3 Boundary Conditions

In fixed frame, the set of governing Eqs. (8)−(11) is accompanied by the following hydrodynamics boundary conditions:

(1) At the vessel wall and bottom: $U_i=0$;
(2) At turbine surface: $U_\theta=1$, $U_r=U_a=0$;
(3) At the free surface: $\partial U_i/\partial X_3=\partial k/\partial X_3=\partial \varepsilon/\partial X_3$.

Where $U_\theta$, $U_r$ and $U_a$ represent the tangential, the radial and the axial velocities. They are respectively given by:

$$U_\theta=\frac{-X_2U_1+X_1U_2}{\sqrt{X_1^2+X_2^2}}, U_r=\frac{X_1U_1+X_2U_2}{\sqrt{X_1^2+X_2^2}}, U_a=U_3. \tag{16}$$

### 3.4 Power Number

The power number permits to identify the rate of the power supplied to turbine during it rotation in the stirred vessel. On the other hand, it represents a dimensionless form of the power consumed. The power characteristic is the relation between the power number and Reynolds number. For an agitator of a given geometry, it varies according to the flow regime. The power number is given by:

$$Np=\frac{Po}{\rho N^3 d^5}, \tag{17}$$

where $Po$ denotes the power consumed by the stirred system. It can be calculated using the function of viscous dissipation:

$$Po=\mu\int_{\text{vessel volume}} Q_\nu \, \mathrm{d}\nu. \tag{18}$$

In a dimensionless form, the power number is calculated by:

$$Np=\left(\frac{D}{d}\right)^3\frac{\pi^2}{2Re}\int_{\text{vessel volume}}\overline{Q}_\nu \, \mathrm{d}\,\nu. \tag{19}$$

The function of the dimensionless viscous dissipation is calculated by:

$$\overline{Q}_\nu=\frac{1}{2}\left(\frac{\partial U_i}{\partial X_j}+\frac{\partial U_j}{\partial X_i}\right)^2. \tag{20}$$

## 4 Numerical Method

### 4.1 Numerical Details

The governing Eqs. (8)−(11) accompanied with the boundary conditions are solved using finite volume method. For this purpose, a CFD software based on finite volume method has been retained. It should be noted, that the governing equations are presented in present paper in a fixed reference frame. However, in the case of flows induced by rotating machines, the resolution of the governing system is done in a mobile reference frame in order to simplify the consideration of rotation, especially where these machines do not have cylindrical shapes. Therefore, all equations are rewritten in a moving reference frame.

In the case of an unbaffled vessel, the rotating reference frame (RRF) technique is used. In this approach, the stirrer was kept stationary while the vessel walls were assigned an angular velocity, which is equal and opposite to the impeller rotational velocity.

For the agitated vessels involving baffles or slots, the computational flow has been easily achieved with multiple reference frame (MRF) technique or sliding meshes approaches. For the MRF technique, the computational grid consists of two volume parts: An inner rotating cylindrical volume enclosing the turbine, and an outer, stationary volume containing the rest of the tank. However, the sliding mesh approach divides the computational domain into two meshes, one moving with the impeller and the other one is fixed. Hence, in the present study, the MRF approach has been used to solve the governing system. The domain was discretized using an unstructured tetrahedral mesh refined in the vicinity of the impeller and of the slots, see Figure 2. This allows representing the geometry of the tank forming the computational domain. The finite volume method is conservative. It involves integrating the governing equations over each control volume, which helps in ensuring the conservation of mass, momentum, and other conserved turbulence quantities. The fluxes of the respective quantities across the cell faces are computed, and the production and dissipation terms are evaluated to update the fields for the pressure, velocity components, turbulence kinetic energy ($k$), and turbulence dissipation rate ($\varepsilon$) during each iteration of the solver. This process ensures that the conservation laws and turbulence modeling are properly accounted for in the numerical simulation.

The finite volume discretization approximates the spatial derivatives in the Navier-Stokes equations and the $k$-$\varepsilon$ RANS turbulence equations. The convective and diffusive terms are discretized based on the mesh geometry. The CFD solver used to solve the discrete equations resulting from the finite volume method is implicit. Due to the nature of the present non-linear problem and turbulent flows, implicit solvers employ iterative solution schemes to handle both linear and non-linear terms, while accounting for the regions of the mobile and fixed reference frames considered when using the MRF method for rotating flows. Regarding the non-linear terms, the linearization step allows treating them around the iterative solutions. The discretization of boundary conditions by the finite volume method involves using appropriate numerical approximations for the values of variables or their derivatives on the control faces in the vicinity of the boundary. Specifically, for the Dirichlet conditions, including the axial, tangential, and radial velocities on the boundaries of the tank and the turbine. Regarding the free surface of the tank, the normal gradients of the turbulent kinetic energy, turbulent dissipation rate, and velocities are discretized using finite difference approximations to represent spatial derivatives along the neighboring control faces adjacent to the boundary.

The convergence of the numerical solution refers to the process in which the residual gradually decreases as the solver iterates to solve the equations. The lower level of residual refers to the residual level considered sufficiently low to declare convergence of the results. In the present simulation, this level is on the order of $10^{-7}$, which means the residual must be reduced to a value very close to practically undetectable to achieve convergence. The numerical values remain almost unchanged during the last 4000 iterations of the simulation. This indicates that the solution is stable and that it no longer varies significantly, suggesting adequate convergence.

### 4.2 Mesh Check

In order to confirm the total independence of the different results obtained from the numerical simulations by the finite volume method, a mesh test was necessarily carried out. The procedure is based on the highlighting of several numbers of element in increasing order on the variation of the power number which represents a global characteristic of the agitated system. After the analysis of the variation of the power number values according to three meshes (M1−M3), it was opted for a mesh containing 376680 tetrahedral elements (mesh M2) beyond which the values of the power number remain practically unchanged. Moreover, the time of simulation is not very important compared with the case of the mesh M3, see Table 1.

### 4.3 Code Validation

Before any numerical study, the computational results have to be validated with the experimental or numerical results existing in the literature. In the same geometrical parameters and flow conditions of the experimental work of Wu and Patterson [37] and the numerical work of Feng et al. [38], the procedure of validation has been done in the present paper.

Figure 3(a) shows the variation of the tangential velocity along the height of the tank at a radial position $R^* = 0.185$ and $\theta^* = 0°$. It is clearly shown that the results are in good agreement with those obtained by Wu and Patterson [37]. It is also observed in Figure 3(b) where the variation is taken along of the line $R^* = 0.22$ and $\theta^* = 0°$, that the variations of the radial velocity for a Reynolds

**Table 1** Variation of power number as function of the number of elements

| Mesh | M1 | M2 | M3 |
|---|---|---|---|
| Elements | 210680 | 376680 | 501312 |
| Power number | 5.221 | 5.432 | 5.438 |

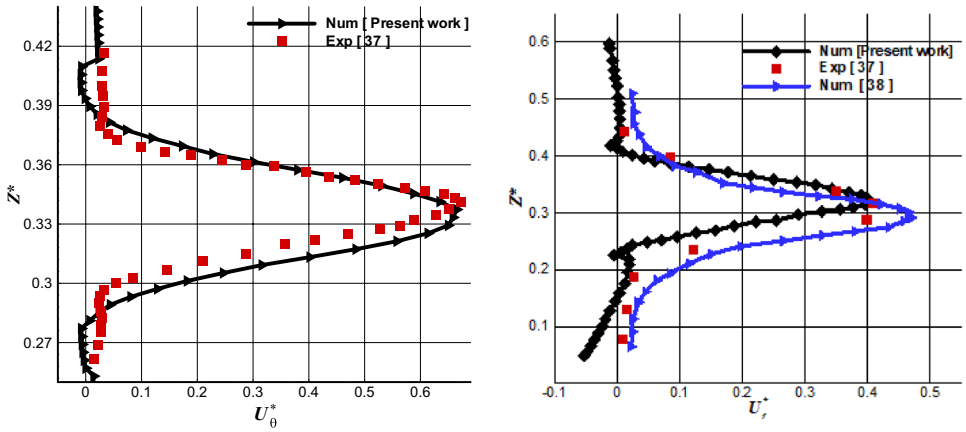


**Figure 3** Comparison between tangential and radial velocities of the present study and those of Refs. [37, 38] at $Re = 4\times10^4$: (**a**) Tangential velocity, (**b**) Radial velocity

**Table 2** Comparison between power number of the present study and those of Refs. [15, 16] for various values of Reynolds number

| Reynolds number | Karcz and major [16] | Foukrach et al. [15] | Present work | Deviation (Exp) (%) | Deviation (Num) (%) |
|---|---|---|---|---|---|
| $Re = 4\times10^4$ | 0.85 | 0.91 | 0.85 | 00.00 | 06.59 |
| $Re = 6.10^4$ | 0.76 | 0.80 | 0.84 | 10.52 | 05.00 |
| $Re = 1\times10^5$ | 0.86 | 0.76 | 0.82 | 04.65 | 07.89 |

number $Re = 4\times10^4$ are in satisfactory congruent with the experimental data [37] and numerical results [38].

Table 2 shows the variation of the power number as function of Reynolds number of the present simulation compared to Refs. [15, 16]. The data presented in this table shows a fairly good agreement between the present results and those of Refs. [15, 16]. It should be noted that, during the comparative evaluation with experimental data, the relative deviation did not exceed 11% [16]. Similarly, for numerical results, the deviation remained below 8% [15]. This observation signifies an excellent validation of the present simulation with the reference. The high level of precision highlights the robustness of the present numerical approach and its exceptional ability to faithfully reproduce the characteristics observed in the experimental data. These results strengthen the present confidence in the relevance of the turbulence model and the rigor of our finite-volume resolution method.

## 5 Results and Discussion

In this section, the results of the numerical simulation of the turbulent flow in the stirred tank equipped with inclined slots are presented. These results are in the form of streamlines, velocity contours as well as curves of the velocity components and the power number. The Reynolds number and the inclination angle of the slots vary respectively in the ranges of $10^4$ to $10^5$ and 0 to 32.5°.

### 5.1 Effect of the Slot Inclination Angle

The flow in the vicinity of the turbine blades promotes the mass and momentum transfer. Turbulence levels are high in the vicinity of the blades, thus the vortex formed below the turbine can reach the free surface of the liquid in the case of vessels without baffles, and gradually decreases in the case of vessels with slots.

The study of Youcefi et al. [29] showed that the slot where $F/D=1/5$ performs the better reduction in the vortex size and in the power number. This work extends the later study, where the configuration of the slots is inclined by an angle $\alpha$.

Figure 4 illustrates the turbulent flow streamlines at the level of the vertical plane of the vessel passing through the turbine blade for different angles of slot inclination, namely the standard case ($\alpha = 0$). It has been clearly observed that the dimension of the vortex formed between the free surface of the flow and the blades of the Rushton turbine decreases as the inclination angle of the slots increases when the rotation of the turbine is effectuated in the negative direction. However, the dimension of this vortex zone increases in the case where the turbine

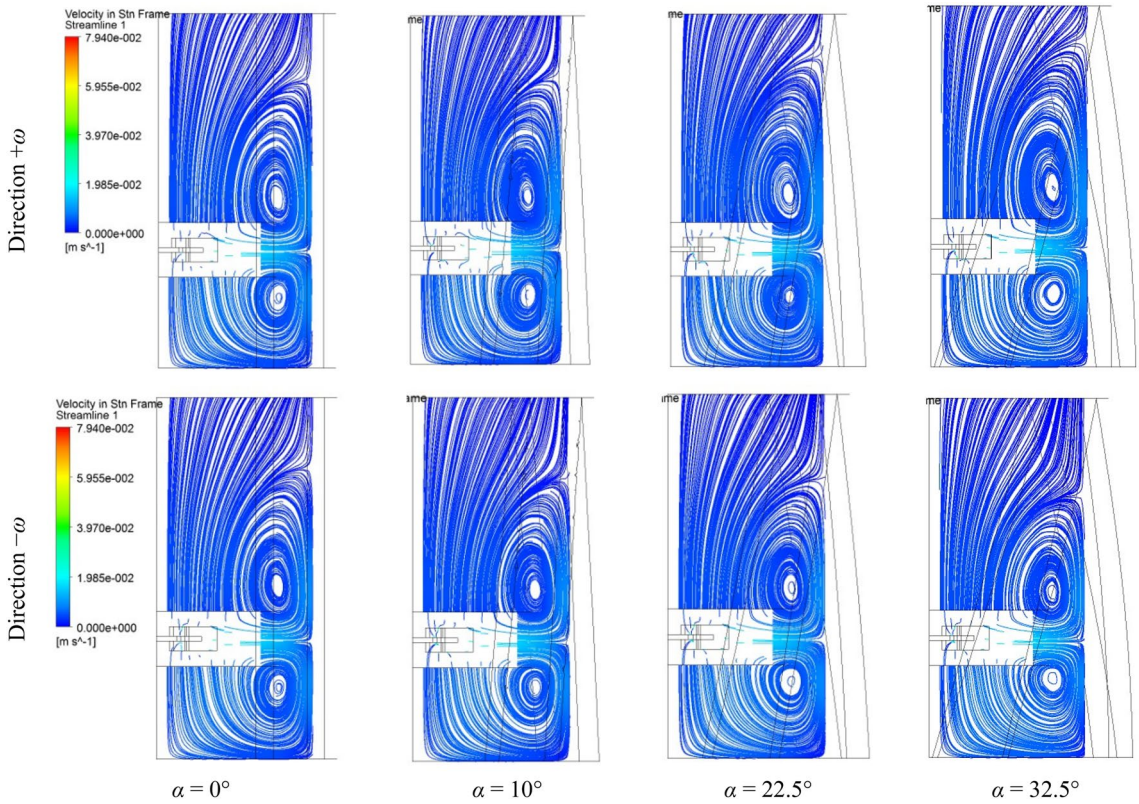


**Figure 4** Streamlines in the vertical plane for different inclination angles and different rotation directions at $Re = 4 \times 10^4$ and $F/D = 1/5$

rotates in the positive flow direction. Indeed, the negative direction of the turbine rotation presents the best choice to reduce the size of the vortex. Nevertheless, the dimension of this vortex in the case of a positive rotation always remains minimal compared to a unbaffled vessel. Regarding the second vortex located between the tank bottom and the turbine blades, it has been observed that regardless of the turbine's rotational direction and the inclination angle of the baffle, its size remains practically unchanged due to the limited influence of the slots in the vicinity of the tank bottom. Therefore, in the subsequent analysis of the results, particular attention will be focused only on the vortex situated between the turbine blades and the free surface.

Table 3 shows a comparison of the vortex length for different configurations including: Unbaffled vessel, baffled vessel and vessel with slots of different inclination angles. In fact, the length of the vortices provides a more significant measure for interpreting the results. They are determined based on the points of change in sign of the axial velocity on the measurement median plane. In the direction $-\omega$, it has been noted that the vortex length decreases with the increase of the inclination angle of the slot by a rate of about 17% for the case of $\alpha = 32.5°$ compared with the standard case. As for the comparison with the baffled vessel, this rate is about 10%.

In the direction $+\omega$, the vortex size augments with the increase of the inclination angle. Nevertheless, it always remains lower compared to the case of a unbaffled tank. Indeed, when the turbine rotates in the direction $-\omega$, the presence of inclined slots has a restraining effect on the vortex size. As the inclination angle of the slot increases, it introduces additional flow restrictions, reducing the available space for vortex development. This leads to a

**Table 3** Variation of the vortex size as function of the slots inclination angle for $Re = 4 \times 10^4$

| **Vessel** | **Unbaffled vessel** | **Baffled vessel** | **Vessel with slots of $F/D = 1/5$** | | | |
|---|---|---|---|---|---|---|
| **Inclination angle** | – | – | $\alpha = 0°$ | $\alpha = 10°$ | $\alpha = 22.5°$ | $\alpha = 32.5°$ |
| Direction $+\omega$ | 0.667 | 0.434 | 0.468 | 0.479 | 0.538 | 0.570 |
| Direction $-\omega$ | 0.667 | 0.434 | 0.468 | 0.440 | 0.427 | 0.391 |

decrease in vortex length compared to both the standard unbaffled case and the baffled vessel. The baffles and slots create flow obstructions that hinder vortex expansion, resulting in a reduction of the vortex length. Conversely, when the turbine rotates in the direction $+\omega$, the vortex size tends to increase with the inclination angle of the slot due to the fluid flow interaction with the inclined slots differently, promoting vortex expansion. The presence of baffles or slots, even when they encourage vortex development, still imposes some restrictions on the vortex size, preventing it from reaching the dimensions seen in an unbaffled configuration.

Figure 5 presents the variation of the axial velocity along the vessel height for different inclination angles $\alpha$ of slots and different rotation velocities $+\omega$ and $-\omega$. It is observed that the axial component of the velocity becomes very weak near the free surface of liquid when using different inclination angles of slots in comparison with unbaffled vessel, which explains the dissipation of vortex in this region of the vessel, see Figure 5(a). On the other hand, it is shown in Figure 5(b) that the free surface of liquid is insignificant for slots inclination angles of $\alpha$ =22.5° and 32.5° compared to the baffled vessel.

In Figure 6, the velocity contours are displayed for a Reynolds number of $Re = 9\times10^4$, considering both rotational directions, $+\omega$ and $-\omega$. The visualization clearly illustrates that regions with higher fluid velocities are predominantly concentrated near the turbine. This observation is expected as the turbine imparts momentum to the fluid, generating higher velocities in its vicinity. The presence of slots in the vessel introduces significant changes in the fluid flow compared to the baffled tank.

Specifically, the slots create a larger shear region, characterized by sharp velocity gradients and increased turbulence. This is a key feature that distinguishes the slotted agitated vessel from the baffled configuration. The larger shear region enhances the fluid mixing and dispersion of different components within the fluid. Moreover, as the inclination angle of the slots increases for both rotational directions, the region of well-stirred fluid expands.

This means that a larger volume of the fluid experiences enhanced mixing, resulting in improved mixing efficiency. The inclination of the slots promotes the generation of additional vertical structures, which further facilitates the mixing process within the vessel. Additionally, the study highlights that the fluid motion in the upper part of the turbine becomes more intense as both the inclination angle $\alpha$ and the rotational direction $+\omega$ increase. This intensification of fluid motion is attributed to the interplay between the turbine's rotational force and the inclined slots' impact on the fluid flow. The inclined slots influence the flow patterns near the upper part of the turbine, leading to intensified fluid motion in that region.

### 5.2 Effect of Inertia

In this section, the effect of Reynolds number ($4\times10^4 \leq Re \leq 9\times10^4$) is highlighted on the hydrody-namic structure inside the slotted agitated vessel. It should be noted, that the inclination angle in this section is set at 32.5°. In fact, the investigation highlights the effect of different rotation speeds on the hydrodynamic behavior inside the slotted stirred tank.

Figure 7 illustrates the flow streamlines inside the slotted agitated vessels at different Reynolds numbers. It has been observed that the Reynolds number has a significant impact on the vortex size (length) for both the

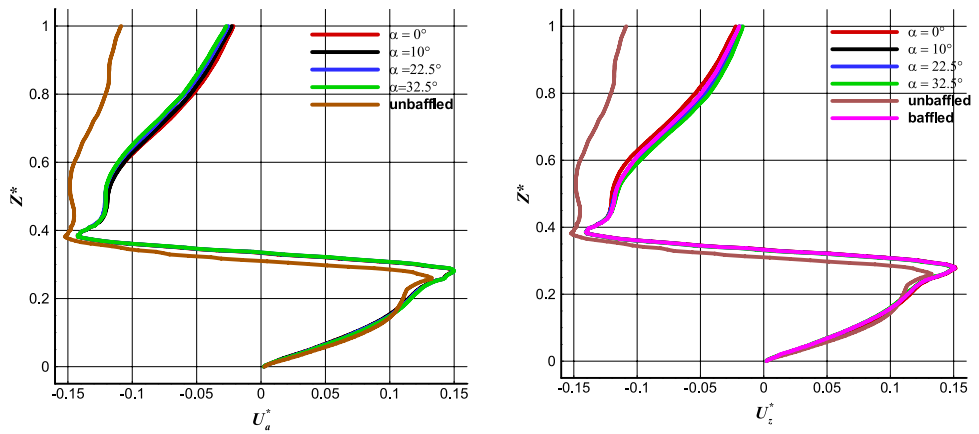


(a) Direction $+\omega$ (b) Direction $-\omega$

**Figure 5** Axial velocity along the vertical line $R^* = 0.185$ for different inclination angles and different rotation directions at $Re = 4\times10^4$ and $F/D = 1/5$

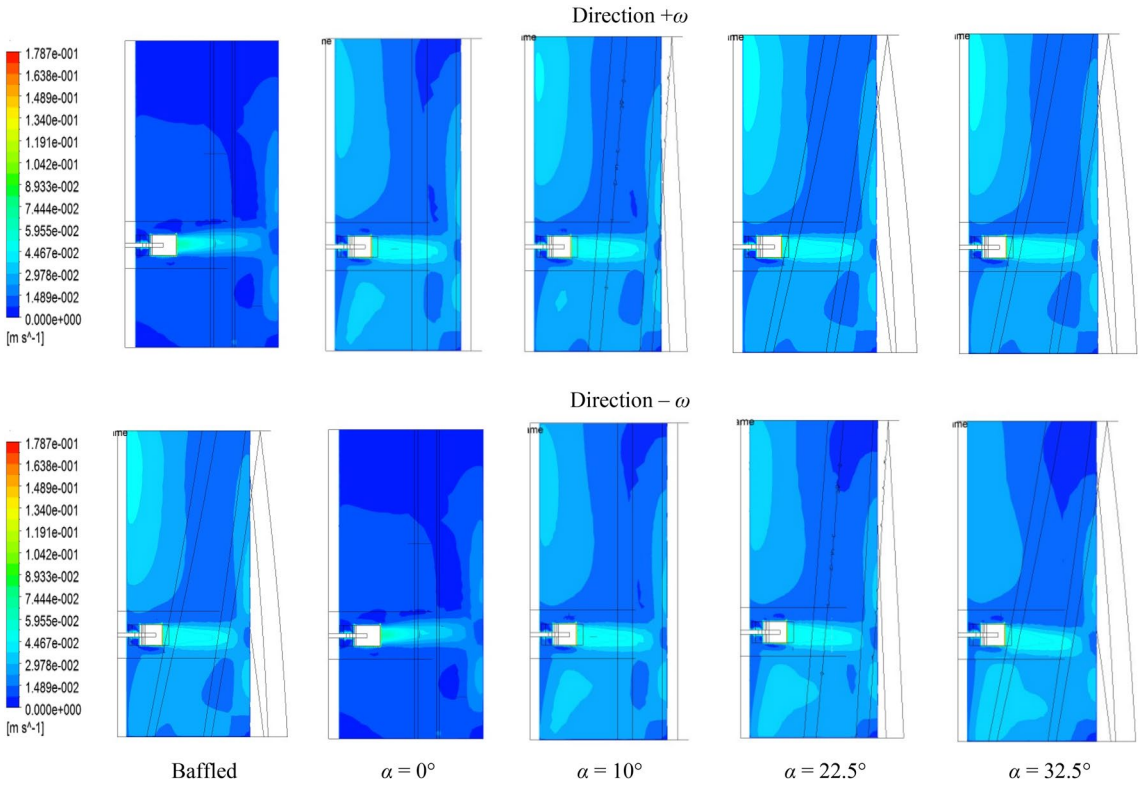


**Figure 6** Velocity contours for different inclination angles and different rotation directions at $Re = 9\times10^4$ and $F/D = 1/5$

positive and negative rotation directions of the turbine. For the positive rotation direction ($+\omega$), as the Reynolds number increases, the vortex size also increases. Higher Reynolds numbers lead to stronger fluid inertia effects, promoting vortex expansion and resulting in larger vortex lengths compared to lower Reynolds numbers. Conversely, for the negative rotation direction ($-\omega$), the vortex length is smaller than that observed for positive rotation. As the Reynolds number increases, the vortex size in the negative rotation direction also increases, but it remains smaller compared to the positive rotation case. The fluid dynamics and flow patterns in the negative rotation direction differ from the positive rotation, leading to different vortex developments. Furthermore, at a specific Reynolds number of $Re = 9\times10^4$, a secondary vortex is observed to form above the primary one. This phenomenon is attributed to the intensification of inertia effects at this high Reynolds number. The stronger fluid inertia creates additional vertical structures in the flow, resulting in the formation of a secondary vortex above the primary one. In this case, the fluid experience significant velocity gradients, especially near the free surface. These velocity gradients lead to substantial shear and regions of increased vorticity, resulting in the formation of the secondary vortex.

The presented data in Table 4 illustrate the relationship between vortex length and the Reynolds number. It represents also the effect of the rotational speed ($\omega$) of the turbine. As the turbine's rotational speed increases, it leads to higher fluid velocities and subsequently larger Reynolds numbers. Similarly, to the figure, the key observation is that as the Reynolds number increases, the vortex length also increases. This suggests that higher Reynolds numbers correspond to more turbulent or complex flow conditions, resulting in longer vortices in the fluid flow field. For instance, the data shows an approximate 18% increase in vortex length when the Reynolds number rises from $Re = 4\times10^4$ to $Re = 9\times10^4$ in two rotation directions. In other words, the observed relationship between vortex size and the Reynolds number is independent of whether the turbine rotates in the $-\omega$ or $+\omega$ direction.

Figure 8 illustrates the distribution of the axial velocity along the vertical line $R^* = 0.266$ for different Reynolds numbers in the two directions of rotation. Evidently, the axial flow become more important with the rise of the inertia forces especially in the upper and the lower parts of the agitated vessel. However, in the vicinity of the turbine blades, the axial flow is quasi-absent due to the dominance of the radial flow in this region. Therefore, the

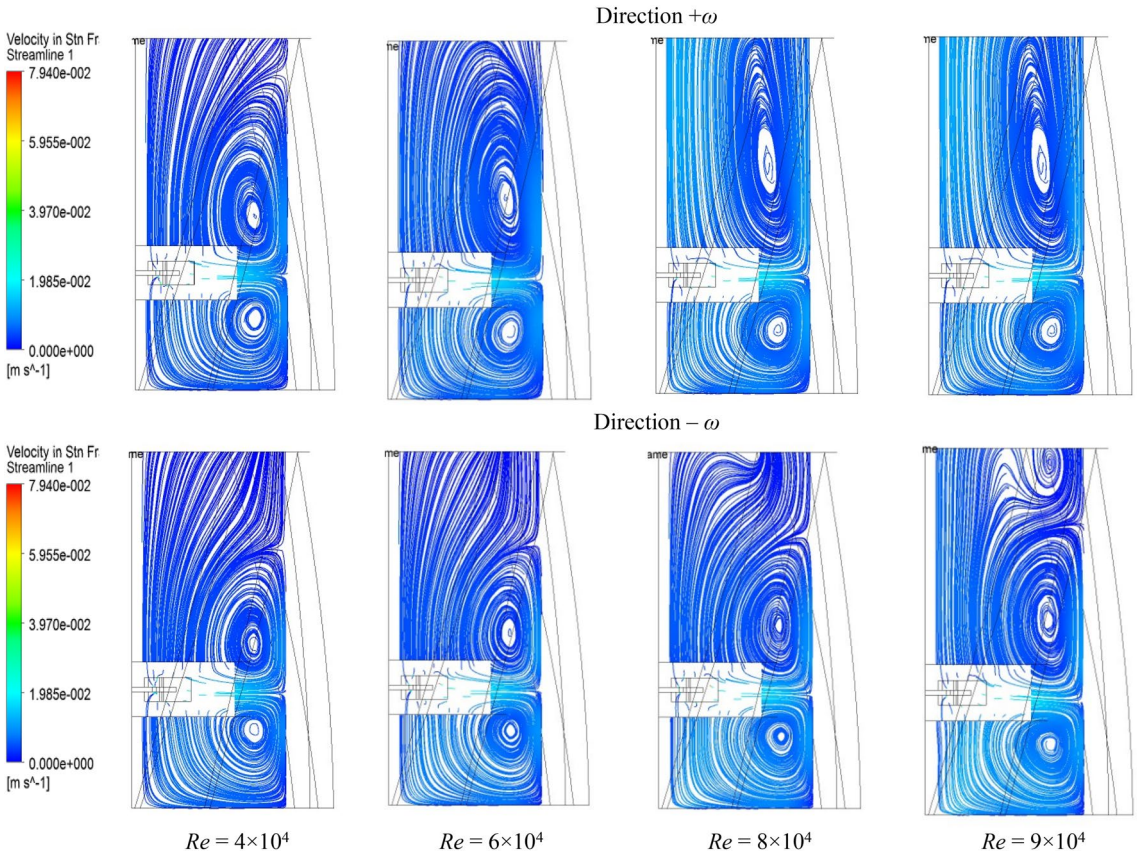


**Figure 7** Streamlines in the vertical plane for different Reynolds numbers and different rotation directions at $\alpha = 32.5°$ and $F/D = 1/5$

**Table 4** Variation of the vortex size as function of Reynolds number for $\alpha = 32.5°$

| Vessel | Vessel with slots of $F/D = 1/5$ | | | |
|---|---|---|---|---|
| **Reynolds number** | $Re = 4\times10^4$ | $Re = 6\times10^4$ | $Re = 8\times10^4$ | $Re = 9\times10^4$ |
| Direction $+\omega$ | 0.570 | 0.667 | 0.667 | 0.667 |
| Direction $-\omega$ | 0.391 | 0.404 | 0.432 | 0.460 |

pumping of the fluid from the turbine blade in the vertical plane is inclined towards the bottom of the tank particularly in the case of $Re = 9\times10^4$, see Figure 9.

### 5.3 Power Consumption

The power number is an important characteristic in studies of mechanical and mixing agitation. It is difficult to find a study in the literature that does not include the determination of this global characteristic. Indeed, the knowledge of the power consumption rate in the present study allows to complete the hydrodynamic aspect and to optimize the different geometrical and/or kinematic parameters for an efficient operation. The results of Table 5 show the effect of the slots inclinations on the power number in the case of $Re = 9\times10^4$.

For the rotation direction $+\omega$, it can be seen that the power number increases as the angle of inclination increases. However, for the rotation direction $-\omega$, the power number decreases with the increase of the inclination angle with a rate of 4.30%. Generally, the use of inclined slots at an angle of 32.5° allows to reduce the power consumption with a rate between 49% and 54% compared to baffled vessel.

For the Reynolds number higher than $4\times10^4$, the power consumption number $Np$ can be reduced for high inclination angles and that for a rotation direction $(-\omega)$. On the other hand, for a rotation direction $(+\omega)$, the power consumption number is proportional to the inclination angle for Reynolds number higher than $Re > 4\times10^4$. It should be noted, that in case of Reynolds number less than $4\times10^4$, the inclination angle of the slots does not affect the energy stat inside the agitated vessel, see Figure 10.

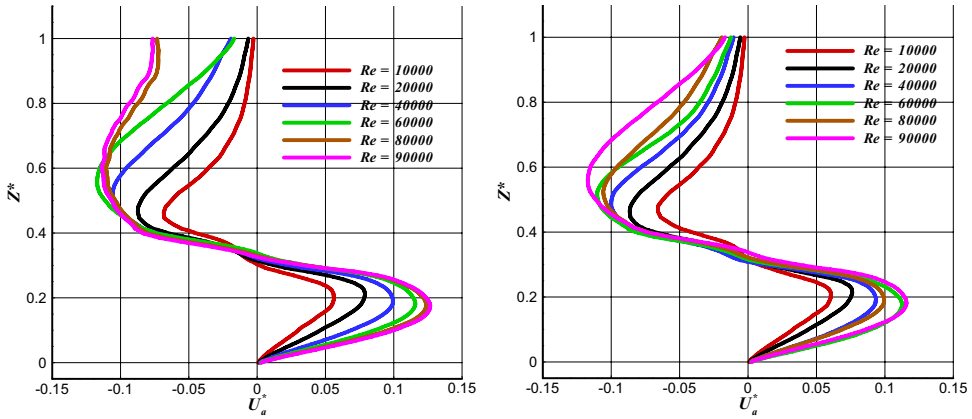


(a) Direction $+\omega$ (b) Direction $-\omega$

**Figure 8** Axial velocity along the vertical line $R^* = 0.266$ for different Reynolds numbers and different rotation directions at $\alpha = 32.5°$ and $F/D = 1/5$

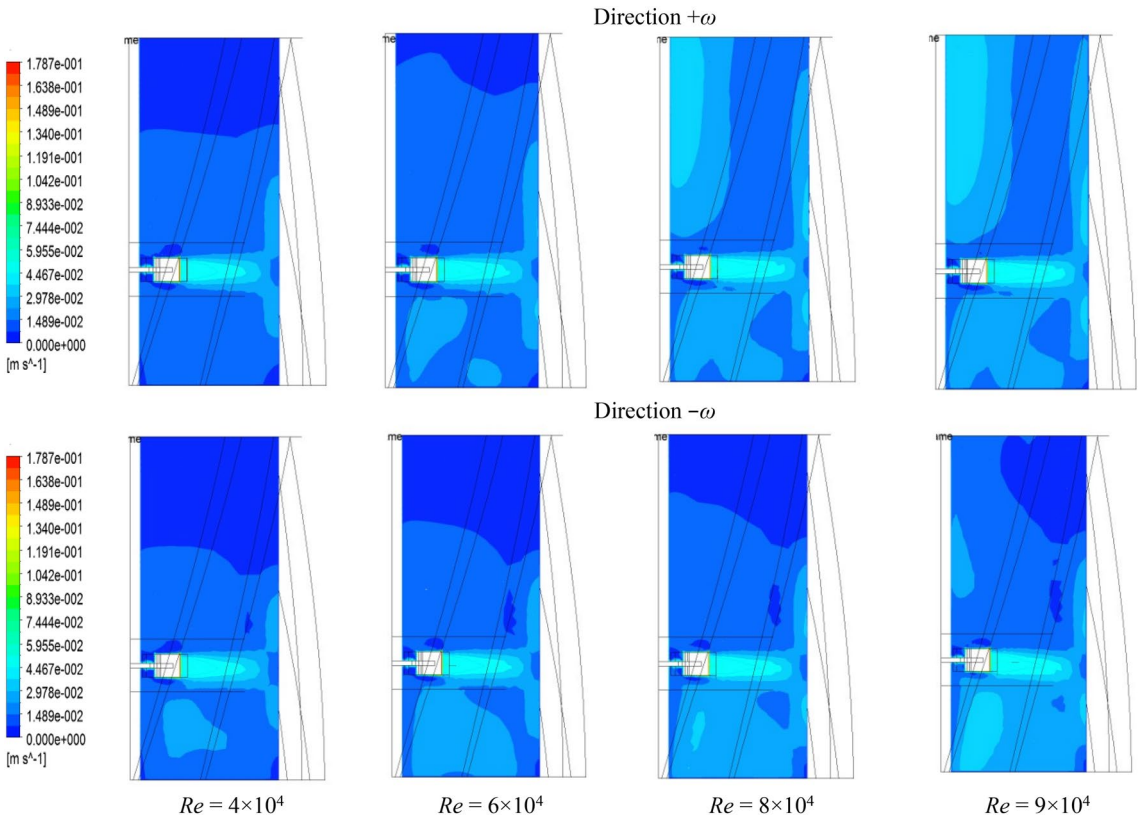


**Figure 9** Velocity contours for different Reynolds numbers and different rotation directions at $\alpha = 32.5°$ and $F/D = 1/5$

**Table 5** Variation of power number as a function of the inclination angle for $Re = 9\times10^4$ and $F/D = 1/5$

| Directions of rotation | $\alpha = 0°$ | $\alpha = 10°$ | $\alpha = 22.5°$ | $\alpha = 32.5°$ | Baffled |
|---|---|---|---|---|---|
| $+\omega$ | 3.25 | 3.30 | 3.34 | 3.38 | 6.71 |
| $-\omega$ | 3.25 | 3.19 | 3.12 | 3.11 | 6.71 |

### 5.4 Best Configuration

In this section, a comparative analysis is presented between different agitated vessels with different inclined slots in terms of vortex size and power consumption. It has been considered to identify the best geometrical configuration allowing to reduce both the vortex size and the power consumption.

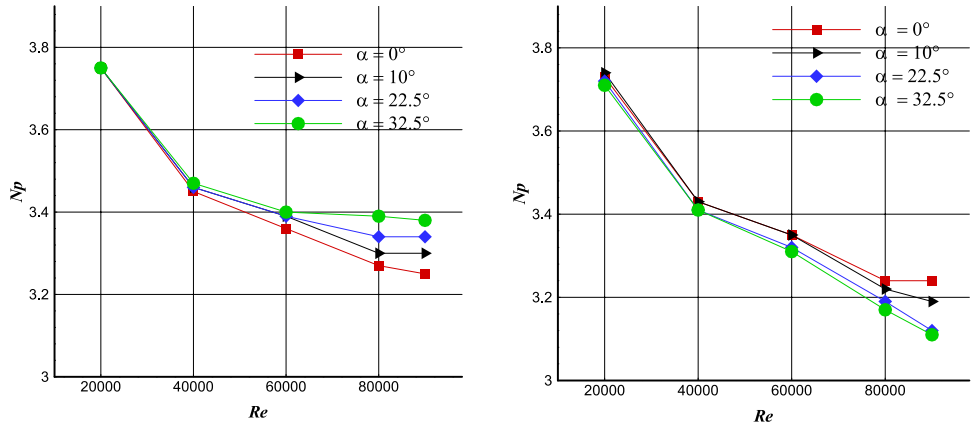


(a) Direction +ω (b) Direction −ω

**Figure 10** Power number as a function of Reynolds number

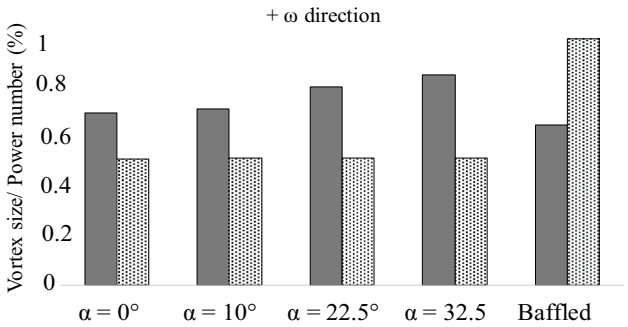


**Figure 11** Histogram of vortex size and power number for different inclinations in +ω direction

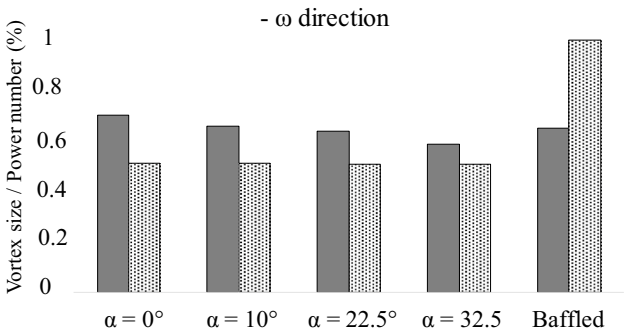


**Figure 12** Histogram of vortex size and power number for different inclinations in −ω direction

It has been shown in the previous sections that the use of inclined slots instead of conventional baffles in agitated vessels reduces the size of the vortex formed between the free surface and the turbine blades when it rotates in the negative direction. On the other hand, the rotation of the turbine in the positive direction does not reduce the size of this vortex. Indeed, as the angle of inclination of the slots increases, the vortex becomes wider. Nevertheless, the power consumption decreases considerably when using inclined slots where the turbine rotates in both directions.

Figures 11 and 12 show the variation of the power number as well as of the vortex size for different geometrical configurations of the slotted agitated tank, including the classically baffled tank in the form of a histogram where the quantities are normalized. The Reynolds number has been set at $Re = 4\times10^4$, however, the slot inclination angles are respectively taken at: $\alpha = 0°$, 10°, 22.5° and 32.5°.

From the histograms of Figure 11, where the turbine rotates in the positive direction, it has been shown that the stirred tank equipped with a straight slot presents the best configuration in terms of power consumption and vortex size. As for the case of a rotation in the negative direction, the stirred tank equipped with inclined slots by an angle of 32.5° presents the best configuration compared to all the previous cases including the case of a classically baffled tank in terms of power and vortex size, see Figure 12. It should be noted that, the slot agitated tank inclined at an angle of 32.5° where the turbine rotates in the negative direction also presents the best configuration in terms of axial velocity, see Figure 13.

## 6 Conclusions

In this paper, a numerical investigation of a Newtonian fluid within an agitated vessel generated by standard Rushton turbine has been carried out. The effects of inclined slots installed in the vessel sidewall on the power consumption and the vortex size have been presented. Through this study, we were able to demonstrate the following important points:

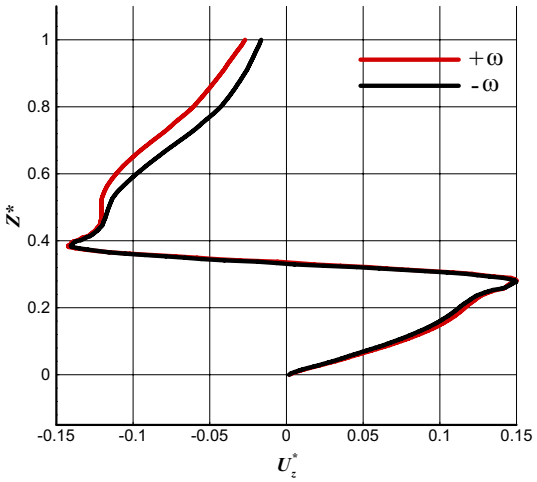


**Figure 13** Axial velocity along the vertical line $R^* = 0.185$ for different Reynolds numbers and different rotation directions at $\alpha = 32.5°$ and $F/D = 1/5$

(1) Introduction of slots in the vessel with a fixed aspect ratio ($F/D = 1/5$) and inclination angles (0°, 10°, 22.5°, and 32.5°) resulted in a significant reduction of approximately 50% in energy consumption compared to the baffled vessel configuration.
(2) The power number exhibited a slight decrease with the increasing inclination angles, specifically following the rotation direction $-\omega$. Indeed, the system displayed lower energy consumption when utilizing an inclination angle of $\alpha = 32.5°$ and the negative rotation direction $-\omega$.
(3) In the case of the negative rotation direction $-\omega$, the vortex size decreases with the increasing inclination angles. It's essential to note that the vortex size, although reduced, remained considerably smaller compared to that observed in baffled and unbaffled vessel configurations.
(4) Based the results and the conception conditions, it can be concluded that the configuration employing slots with an inclination angle of $\alpha = 32.5°$ and the negative rotation direction $-\omega$ represents the optimal stirring system. This configuration aligns well with the design conditions of vessels featuring inclined slots and offers substantial energy savings while maintaining efficient mixing performance.

**Nomenclature**

**Symbol**

| | |
|---|---|
| $a$ | Blade length (m) |
| $b$ | Shaft diameter (m) |
| $c$ | Clearance impeller bottom (m) |
| $C\varepsilon_1$ | Turbulent coefficient |
| $C\varepsilon_2$ | Turbulent coefficient |
| $D$ | Tank diameter (m) |
| $d$ | Impeller diameter (m) |
| $E$ | Slot depth (m) |
| $F$ | Circumference slot (m) |
| $Fr$ | Froude number |
| $g$ | Gravity acceleration (m/s$^2$) |
| $H$ | Tank height (m) |
| $h$ | Blade height (m) |
| $k$ | Turbulent kinetic energy (m$^2$/s$^2$) |
| $N$ | Impeller rotation speed (1/s) |
| $Np$ | Power number |
| $P$ | Dimensionless pressure |
| $p$ | Pressure (Pa) |
| $P_k$ | Turbulent expression (Pa/s) |
| $Po$ | Power (W) |
| $Qv$ | Viscous dissipation function (1/s$^2$) |
| $Re$ | Reynolds number |
| $t$ | Time (s) |
| $th$ | Disc thickness (m) |
| $U$ | Dimensionless velocity |
| $u$ | Velocity (m/s) |
| $X$ | Dimensionless cartesian coordinate |
| $x$ | Cartesian coordinate (m) |

**Greek**

| | |
|---|---|
| $\alpha$ | Inclination angle |
| $\delta$ | Disc diameter (m) |
| $\varepsilon$ | Turbulent dissipation rate (m$^2$/s$^3$) |
| $\mu$ | Viscosity (Pa.s) |
| $\rho$ | Density (kg/m$^3$) |
| $\sigma_k$ | Turbulent coefficient |
| $\sigma_\varepsilon$ | Turbulent coefficient |
| $\tau$ | Dimensionless time |
| $\omega$ | Impller rotation speed (1/s) |

**Subscript**

| | |
|---|---|
| $a$ | Axial direction |
| $i, j$ | Cartesian direction indexes |
| $r$ | Radial coordinate |
| $t$ | Turbulent |
| $\theta$ | Tangential coordinate |

**Superscript**

| | |
|---|---|
| $-, *$ | Dimensionless function |

**Authors' Contributions**

SY performed the numerical simulation, presented the numerical details and analyzed the results; MB proposed the idea of the paper and controlled the results interpretation; AY performed the paper methodology and assisted in interpreting the numerical results; AM proofread, revised, and structured the article. All authors read and approved the final manuscript.

**Authors' Information**

Sarra Youcefi born in 1987 in *Oran, Algeria*, is a senior lecturer at *University of Sciences and Technology of Oran, Algeria*. She received her PhD degree in mechanical engineering in 2013, from *University of Sciences and Technology of Oran, Algeria*. Her research interests include agitation system and fluid mechanics.

Mohamed Bouzit born in 1966 in *Bordj-Bou Arreridj, Algeria*, is a professor at *University of Sciences and Technology of Oran, Algeria*. He received his PhD degree from *University of Sciences and Technology of Oran, Algeria,* in 2007. His area of research includes fluid flows, heat transfer, magnetohydrodynamics and fluid-structure interactions.
Abdelkader Youcefi born in 1953 in *Chlef, Algeria,* is a professor at *Mechanical Faculty of Engineering, University of Sciences and Technology of Oran, Algeria*. He received his PhD degree from *IMF-Toulouse, France,* in 1993. His area of research includes mixing, fluid and rheology.
Abderrahim Mokhefi born in 1992 in *Oran, Algeria*, is a senior lecturer at *National Polytechnic School of Oran, Algeria*. He received his PhD degree in energetic mechanics from *Tahri Mohamed University of Bechar, Algeria,* in 2022. His current research interests are mainly in the field of computational fluid dynamics, heat transfer, nanofluids electromagnetic and field theory.

**Funding**
No applicable.

## Declarations

**Competing Interests**
The authors declare no competing financial interests.

Received: 25 July 2022 Revised: 7 November 2023 Accepted: 14 November 2023
Published online: 06 December 2023

**References**

[1] S Nagata. *Mixing: principles and applications*. New York: Halsted Press, 1975.
[2] C Xuereb, M Poux, J Bertrand. *Agitation et mélange. Aspects fondamentaux et applications industrielles*. France: Dunod, 2006.
[3] J Bertrand. *Agitation de fluides visqueux. Cas de mobiles à pales, d'ancres et de barrières*. Doctoral dissertation, Toulouse, INPT, France, 1983.
[4] A Youcefi. *Étude expérimentale de l'écoulement d'un fluide visco-élastique autour d'un agitateur bipale en cuve agitée.* Doctoral dissertation, Toulouse, INPT, France, 1993.
[5] H Ameur. Effect of some parameters on the performance of anchor impellers for stirring shear-thinning fluids in a cylindrical vessel. *Journal of hydrodynamics*, 2016, 28(4): 669-675. https://doi.org/10.1016/S1001-6058.
[6] K Ng, M Yianneskis. Observations on the distribution of energy dissipation in stirred vessels. *Chemical Engineering Research and Design*, 2000, 78(3): 334341. https://doi.org/10.1205/026387600527446.
[7] R Zadghaffari, J S Moghaddas, J Revstedt. Large-eddy simulation of turbulent flow in a stirred tank driven by a Rushton turbine. *Computers and Fluids*, 2010, 39(7): 1183-1190. https://doi.org/10.1016/j.compfluid.2010.03.001.
[8] A Mokhefi, M Bouanini, M Elmir. Numerical simulation of laminar flow and heat transfer of a non-Newtonian nanofluid in an agitated tank. *International Journal of Heat and Technology*, 2021, 39(1): 251-261. https://doi.org/10.18280/ijht.390128.
[9] A Mokhefi, M Bouanini, M Elmir, et al. Effect of an anchor geometry on the hydrodynamic characteristics of a nanofluid in agitated tank. *Defect and Diffusion Forum*, 2021, 409: 179–193. https://doi.org/10.4028/www.scientific.net/DDF.409.179.
[10] A Mokhefi, M Bouanini, M Elmir et al. Effect of the wavy tank wall on the characteristics of mechanical agitation in the presence of a Al2O3-water nanofluid. *Metallurgical and Materials Engineering*, 2021, 27(3): 301-320. https://doi.org/10.30544/626.
[11] A Mokhefi, M Bouanini, M Elmir, et al. Numerical investigation of mixed convection in an anchor-stirred tank filled with an Al2O3-water nanofluid. *Chemical Papers*, 2022, 76(2): 1-19. https://doi.org/10.1007/s11696-021-01914-2.
[12] S Wang, D V Boger, J Wu. Energy efficient solids suspension in an agitated vessel-water slurry. *Chemical Engineering Science*, 2012, 74: 233-243. https://doi.org/10.1016/j.ces.2012.02.035.
[13] S Youcefi, A Youcefi. Power consumption and mixing time in rheologically complex fluids by a two-bladed impeller. *Journal of Mechanical Science and Technology*, 2015, 29(2): 543-548.
[14] M Taghavi, R Zadghaffari, J Moghaddas, et al. Experimental and CFD investigation of power consumption in a dual Rushton turbine stirred tank. *Chemical Engineering Research and Design*, 2011, 89(3): 280-290. https://doi.org/10.1016/j.cherd.2010.07.006.
[15] M Foukrach, M Bouzit, H Ameur et al. Effect of agitator's types on the hydrodynamic flow in an agitated tank. *Chinese Journal of Mechanical Engineering*, 2020, 33(1): 1-18. https://doi.org/10.1186/s10033-020-00454-2.
[16] J Karcz, M Major. An effect of a baffle length on the power consumption in an agitated vessel. *Chemical Engineering and Processing: Process Intensification*, 1998, 37(3): 249-256.
[17] K Yapici, B Karasozen, M Schafer et al. Numerical investigation of the effect of the Rushton type turbine design factors on agitated tank flow characteristics. *Chemical Engineering and Processing*, 2008, 47(8): 1340-1349. https://doi.org/10.1016/j.cep.2007.05.002
[18] M Beloudane, M Bouzit, H Ameur. Numerical investigation of the turbulent flow generated with a radial Turbine using a converging hollow blade. *Polish Journal of Chemical Technology*, 2018, 20(4): 129-137. https://doi.org/10.2478/pjct-2018-0065
[19] S Hassouni, H Laidoudi, O Makinde et al. A qualitative study of mixing a fluid inside a mechanical mixer with the effect of thermal buoyancy. *Archives of Thermodynamics*, 2023, 44(1): 105-119. https://doi.org/10.24425/ather.2023.145879.
[20] Z Jia, L Xu, X Duan, et al. CFD simulation of flow and mixing characteristics in a stirred tank agitated by improved disc turbines. *Chinese Journal of Chemical Engineering*, 2022, 50: 95-107.
[21] I Jenish, M Appadurai, E F I Raj. CFD Analysis of modified Rushton turbine impeller. *Int. J. Sci. Manag. Stud. (IJSMS)*, 2021, 4: 8–13. https://doi.org/10.51386/25815946/ijsms-v4i3p102.
[22] Y Zhang, Z Gao, Z Li, et al. Transitional flow in a Rushton turbine stirred tank. *AIChE Journal*, 2017, 63(8): 3610-3623. https://doi.org/10.1002/aic.15809.
[23] S Roy, S Acharya. Scalar mixing in a turbulent stirred tank with pitched blade turbine: Role of impeller speed perturbation. *Chemical Engineering Research and Design,* 2012, 90(7): 884-898.
[24] M Ammar, Z Driss, W Chtourou et al. Effects of baffle length on turbulent flows generated in stirred vessels. *Central European Journal of Engineering*, 2011, 1(4): 401-412.
[25] K Bittins, P Zehner. Power and discharge numbers of radial-flow impellers. Fluid-dynamic interactions between impeller and baffles. *Chemical Engineering and Processing,* 1994, 33(4): 295-301. https://doi.org/10.1016/0255-2701 (94)01011-0.
[26] S Bhattacharya, D Hebert, S M Kresta. Air entrainment in baffled stirred tanks. *Chemical Engineering Research and Design*, 2007, 85(5A): 654-664. https://doi.org/10.1205/cherd06184.
[27] Y Fan, J Sun, J Jin, et al. Effects of baffle on flow structure and cyclic variation in stirred tanks with Rushton turbine. *AIP Advances*, 2022, 12(1). https://doi.org/10.1063/5.0073821.
[28] A Tamburini, A Brucato, M Ciofalo, et al. CFD simulations of early-to fully-turbulent conditions in unbaffled and baffled vessels stirred by a Rushton turbine. *Chemical Engineering Research and Design*, 2021, 171: 36-47. https://doi.org/10.1016/j.cherd.2021.04.021.
[29] S Youcefi, M Bouzit, H Ameur, et al. Effect of some design parameters on the flow fields and power consumption in a vessel stirred by a Rushton turbine. *Chemical and Process Engineering*, 2013, 34(2): 293-307. https://doi.org/10.2478/cpe-2013-0024.
[30] M O Shabani, A Mazahery, M Alizadeh, et al. Computational fluid dynamics (CFD) simulation of effect of baffles on separation in mixer settler. *International Journal of Mining Science and Technology*, 2012, 22(5): 703-706. https://doi.org/10.1016/j.ijmst.2012.08.019.
[31] Y Kamla, M Bouzit, A Hadjeb, et al. CFD study of the effect of baffles on the energy consumption and the flow structure in a vessel stirred by a Rushton turbine. *MECHANIKA*, 2016, 22(3): 190-197. https://doi.org/10.5755/j01.mech.22.3.12663.

[32] Y Kamla, M Bouzit, H Ameur, et al. Effect of the Inclination of baffles on the power consumption and fluid flows in a vessel stirred by a Rushton turbine. *Chinese Journal of Mechanical Engineering*, 2017, 30(4): 1008–1016. https://doi.org/10.1007/s10033-017-0158-5.
[33] M Foukrach, H Ameur. Effect of baffles shape on the flow patterns and power consumption in stirred vessels. *SN Applied Sciences*, 2019, 1: 1–11. https://doi.org/10.1007/s42452-019-1550-9.
[34] L Liangchao, C Ning, X Kefeng, et al. CFD study on the flow field and power characteristics in a rushton turbine stirred tank in laminar regime. *International Journal of Chemical Reactor Engineering*, 2019, 17(11): 20180215. https://doi.org/10.1515/ijcre-2018-0215.
[35] V Boonkanokwong, R P Frank, P Valliappan, et al. Flow of granular materials in a bladed mixer: Effect of particle properties and process parameters on impeller torque and power consumption. *Advanced powder technology*, 2018, 29(11): 2733-2752. https://doi.org/10.1016/j.apt.2018.07.022.
[36] X Xiong, Z Liu, C Tao, et al. Reduced power consumption in stirred vessel with high solid loading by equipping punched baffles. *Chinese Journal of Chemical Engineering*, 2023, 56: 203–214. https://doi.org/10.1016/j.cjche.2022.07.018.
[37] H Wu, G K Patterson. Laser-Doppler measurements of turbulent flow parameters in a stirred mixer. *Chemical engineering science*, 1989, 44(10): 2207-2221. https://doi.org/10.1016/0009-2509(89)85155-3.
[38] X Feng, J Cheng, X Li et al. Numerical simulation of turbulent flow in a Baffled stirred tank with an explicit algebraic stress model. *Chemical Engineering Science,* 2012, 69(1): 30-44. https://doi.org/10.1016/j.ces.2011.09.055.